

# Accurate Estimation of Brillouin Frequency Shift in Brillouin Optical Correlation Domain Analysis

K. Yaswanth<sup>†</sup>, *Student Member, IEEE*, Bhargav Somepalli<sup>†</sup>, *Member, OSA*, Uday K. Khankhoje, *Senior Member, IEEE*, Deepa Venkitesh, *Senior Member, OSA*, and Balaji Srinivasan, *Senior Member, OSA*

**Abstract**—Estimation of the accurate value of Brillouin frequency shift (BFS) in a Brillouin optical correlation domain analysis (BOCDA) is challenging due to the contributions to the Brillouin gain spectrum (BGS) from the locations other than corresponding to the correlation between the pump and the probe. In this scenario, we demonstrate optimal post-processing algorithms to retrieve the BFS accurately. We first demonstrate a linear approximation based approach to estimate the BFS with an accuracy of  $< 1$  MHz. This approach needs to be modified for situations where simultaneous sensing is carried out from two or more locations, or with lock-in detection methods. A gradient descent method is proposed and demonstrated in such cases where the component corresponding to the second harmonic of the modulation frequency is used to optimally recover BFS. The method is tested for its performance at different locations of correlation peaks and for perturbation frequency range of  $> 500$  MHz, under different SNR conditions. The error in estimation is found to be less than 1.7 MHz across the entire frequency range for an SNR as low as 5 dB. The algorithm is also validated by comparison with experimental data. The proposed algorithm effectively increases the range and sensitivity of measurement for BFS estimation even when multiple locations are monitored simultaneously.

**Index Terms**—Fiber optic sensors, stimulated Brillouin scattering, gradient descent method.

## I. INTRODUCTION

**D**ISTRIBUTED fiber optic sensors based on stimulated Brillouin scattering (SBS) have been extensively investigated and implemented in the past few decades for monitoring of strain and temperature [1]–[5]. Specifically, sensors based on Brillouin optical correlation domain analysis (BOCDA) have been effectively used for dynamic strain sensing applications [6], [7]. In BOCDA, both the pump and the probe are frequency modulated (FM) and are counter propagated in the fiber under test (FUT) thereby limiting the Brillouin interaction between the two lightwaves to specific locations—referred to as correlation peaks [8], [9]. As in the case of any Brillouin sensor, the accuracy of the measurand in BOCDA depends on the accuracy with which the Brillouin frequency shift (BFS) is determined. Typically, the BFS is estimated from

the peak of the Brillouin gain spectrum (BGS), which ideally is Lorentzian in shape with a 3-dB width of 30 MHz [10]. However, the measured BGS in BOCDA has contributions from the transient Brillouin interactions at locations other than those of correlation peaks as well, resulting in an undesirable background signal which manifests as a broadened spectrum (of width up to 100 MHz) for smaller values of strain changes at the correlation location [11]. Traditional curve fitting algorithms, when applied over a small range of frequencies around the peak may be sufficient to correctly estimate the BFS for cases corresponding to smaller strain perturbations. However, when the BFS at the correlation peak location is very different from that at non-correlation locations (corresponding to a larger applied strain), the undesirable background component dominates, resulting in a large error in the estimated BFS. As a result, the maximum measurable strain in a conventional BOCDA system is limited [12].

Several techniques have been proposed to eliminate the undesirable background signal. In 2006, Song *et al.* proposed and demonstrated a scheme using an intensity modulator introduced at the output of the narrow linewidth light source [12]. In this scheme, the different intensity modulation waveforms are tested and an optimum configuration is experimentally demonstrated where the signal-to-noise ratio at the sensing position is improved by more than 40%. In 2012, Jeong *et al.* implemented a differential measurement scheme with the inclusion of a phase modulator to suppress the background noise thereby increasing the maximum measurable strain [11]. In this scheme, a five-fold enhancement in the spatial resolution is demonstrated compared to a conventional BOCDA system. While these techniques have yielded favorable results, they either add complexity to the sensing system or increase the measurement time. Ideally, the above problem can be addressed using a suitable post-processing algorithm which eliminates the effect of undesirable components in the pump-probe beat spectrum. Specifically, the implementation of a precise post-processing algorithm for BFS estimation can avoid the excessive number of measurements used in differential measurement scheme. We recently proposed an algorithm to accurately determine the BFS based on a simple mathematical model assuming small gain approximation and modeling the SBS interaction as a system of linear equations [13]. Using this algorithm, we demonstrated an accurate estimation of BFS over a large range of values at the correlation peak location through simulations and validated the same through controlled experiments [13].

In this paper, we propose a robust algorithm based on the

<sup>†</sup>Contributed equally to this work

K. Yaswanth, U. K. Khankhoje, D. Venkitesh and B. Srinivasan are with the Department of Electrical Engineering, Indian Institute of Technology Madras, Chennai, India (e-mail: yaswanthkalepu@gmail.com; uday@ee.iitm.ac.in; deepa@ee.iitm.ac.in; balajis@ee.iitm.ac.in).

B. Somepalli was with the Department of Electrical Engineering, Indian Institute of Technology Madras, Chennai, India. He is now with Photonics Research Centre, Department of Electronic and Information Engineering, The Hong Kong Polytechnic University, Hong Kong (e-mail: bhargav.somepalli@polyu.edu.hk).

gradient descent method for accurate estimation of BFS at the correlation peak location. In doing so, we extend our earlier, linear approximation based work, which was found to yield erroneous values when multiple locations within the FUT are monitored using measured data at a harmonic of the modulation frequency [14].

The paper is organized as follows. The numerical modeling of BOCDA system is explained in Section 2. The linear approximation approach for accurate estimation of BFS in BOCDA and the corresponding results are discussed in Section 3 followed by the discussion on the gradient descent method for BFS estimation in Section 4. The simulation results on the implementation of the algorithm and validation with experimental data are discussed in the same section. This is followed by conclusions from this work.

## II. MODELING OF BRILLOUIN OPTICAL CORRELATION DOMAIN ANALYSIS

### A. Overview of BOCDA

In BOCDA technique, a frequency-modulated narrow linewidth laser source is split into pump and probe lightwaves and counter propagated within the FUT [8]. Due to the frequency modulation, the interaction between the two lightwaves is localized at specific locations within the FUT where they form correlation peaks [9]. The measured BGS using a BOCDA system is a two dimensional convolution integral between local BGS with a Lorentzian shape (typically 30 MHz FWHM, with a peak at around 11 GHz for operating wavelength of 1550 nm in case of standard single mode fiber) and pump-probe beat spectrum expressed as [15]

$$g(z_0, f_d) = \frac{P}{A_{eff}} \int_{z=0}^L \int_{-\infty}^{\infty} g_B(z, f) S_b(z_0 - z, f_d - f) df dz, \quad (1)$$

where  $g(z_0, f_d)$  is the normalized Brillouin gain contributed by the correlation peak at position  $z_0$  corresponding to a pump-probe frequency offset of  $f_d$ ,  $P$  is the average pump power,  $A_{eff}$  is the effective area of the fiber at the operating wavelength,  $g_B$  is the local Brillouin gain and  $S_b$  is the pump-probe beat spectrum. The measured Brillouin gain spectrum ( $P_{BGS}(f_d)$ ) is a function of  $f_d$  and is proportional to  $\exp(g(z_0, f_d))$ .

Fig. 1 shows a typical beat spectrum between pump and probe in BOCDA for an FUT of length 1 km with BFS of 10.8 GHz and the correlation peak is positioned at 500 m. Even though the peak of the beat spectrum is located at 500 m, it is non-zero at neighboring locations due to the periodic nature of the frequency modulation [16]. As a result, the measured BGS has contributions from these locations; the resulting BGS would be broader. Even though the power levels of the beat spectrum at locations other than the correlation peak are small, the integrated gain over the entire length and the frequency range could be large. For a given  $P_{BGS}(f_d)$ , the objective is to find the local Brillouin gain,  $g_B$ , at the correlation peak position  $z_0$ .

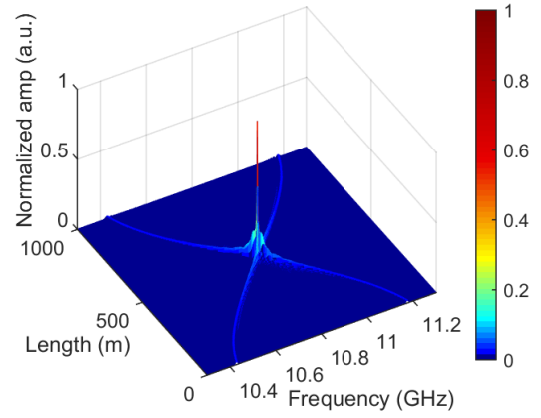


Fig. 1. Beat spectrum between pump and probe showing a peak at correlation peak position along with non-zero amplitude at non-correlation locations.

### B. Numerical model of BOCDA

In order to numerically model the BOCDA system, SBS interaction between pump and probe is considered using steady-state equations [17]. Under undepleted pump approximation and assuming identical polarization states for the pump and probe during interaction, the amplified probe at an offset frequency  $f_d$  from the pump and at any given location,  $z$  in the fiber at time  $t$  is expressed in terms of the incident probe and Brillouin gain as follows.

$$P_{probe}(z, t, f_d) = P_{probe}(z + dz, t - dt, f_d) \times \exp \left\{ g_B(z, t, f_d) \frac{P_{pump}(z, t)}{A_{eff}} dz \right\}, \quad (2)$$

where  $dz$  and  $dt$  are space and time step sizes respectively,  $P_{pump}(z, t)$  is the instantaneous pump power and  $g_B$  is the local Brillouin gain given by [18]

$$g_B(z, t, f_d) = \frac{g_0}{1 + \left( \frac{f_B(z) - f(z, t, f_d)}{\Delta\nu_B/2} \right)^2}, \quad (3)$$

where  $g_0$  is the peak Brillouin gain,  $\Delta\nu_B$  is the Brillouin gain bandwidth and  $f_B$  is the BFS, which is a function of spatial location.  $f(z, t, f_d)$  is the beat frequency between pump and probe at specific  $z$  and  $t$  given by  $f(z, t, f_d) = f_{pp} - f_{pr}$  where  $f_{pp}$  and  $f_{pr}$  are instantaneous frequencies of pump and probe respectively at any specific location,  $z$  in the fiber given by

$$f_{pp}(z, t) = f_c + \Delta f \sin \left( 2\pi f_m \left( t - \frac{z}{v_g} \right) \right), \quad (4)$$

$$f_{pr}(z, t, f_d) = f_c - f_d + \Delta f \sin \left( 2\pi f_m \left( t - \frac{L - z}{v_g} \right) \right), \quad (5)$$

where  $f_c$  represents optical carrier frequency,  $f_m$  is the modulation frequency,  $\Delta f$  is the frequency deviation,  $L$  is the length of the sensing fiber and  $v_g$  is the group velocity of light in fiber. Note that  $z = 0$  is the point where the pump is launched into the fiber.

The probe which is counter propagated with respect to pump, is amplified all along the sensing fiber depending on the instantaneous pump power and the Brillouin gain. The power

of the amplified probe measured at the pump end of the fiber can be written as

$$P_{probe}(0, t, f_d) = P_{probe}(L, t - T) \times \exp \left[ \left\{ g_B(L - dz, t - T + dt, f_d) \times P_{pump}(L - dz, t - T + dt) + \dots + g_B(0, t, f_d) P_{pump}(0, t) \right\} \frac{dz}{A_{eff}} \right] \quad (6)$$

where  $T$  is the time taken for the probe to propagate through the sensing fiber.

Since the Brillouin interaction between the pump and the probe occurs predominantly within the spatial distance corresponding to the correlation peak, it is reasonable to assume that the aggregate gain is small and hence the exponential in Eq. (6) can be approximated to first order terms ( $\exp(x) \approx 1 + x$ ). As a result, the amplified probe power can be expressed as

$$P_{probe}(0, t, f_d) = P_{probe}(L, t - T) \times \left[ 1 + \left\{ g_B(L - dz, t - T + dt, f_d) \times P_{pump}(L - dz, t - T + dt) + \dots + g_B(0, t, f_d) P_{pump}(0, t) \right\} \frac{dz}{A_{eff}} \right] \quad (7)$$

The measured BGS ( $P_{BGS}(f_d)$ ) is typically the DC component of the above relation [19], whose magnitude is decided by the specific frequency offset between pump and probe and can be written as

$$P_{BGS}(f_d) = \sum_{t=dt}^{T_m} P_{probe}(0, t, f_d), \quad (8)$$

where  $T_m (= 1/f_m)$  is the period of the frequency modulation of pump/probe. In the forward simulation model,  $P_{BGS}$  is numerically computed for different pump-probe frequency offsets ( $f_d$ ) in order to emulate the BGS measured using a BOCDA system. A technique to estimate the local Brillouin gain  $g_B$  from the measured BGS based on the above linear approximation is discussed in the following section.

### III. LINEAR APPROXIMATION APPROACH TO ESTIMATE BFS

In order to extract the local Brillouin gain and estimate BFS at the correlation location accurately, we make use of Eqs. (7) and (8). From the BGS measured under specific experimental conditions, all the parameters in Eqs. (7) and (8) such as modulation frequency, maximum frequency deviation and length of the fiber are known *a priori*, except the BFS  $f_B$  at the correlation location. Hence, by writing the equations for all the pump-probe frequency offsets and knowing the BGS at locations where the correlation is not intended, we can formulate a system of linear equations to estimate the Brillouin gain  $g_B$  at the correlation location, and thereby determine the BFS.

#### A. BFS estimation for different BFS values at correlation location

In order to validate the BFS estimation using the above linear approximation, the measured BGS is simulated with the following parameters. The length of the FUT considered is 1 km with a delay fiber of  $\sim 13.3$  km, although the above algorithm is agnostic to the sensing fiber length. The modulation frequency ( $f_m$ ) used is 70.4 kHz which generates a correlation peak at 50 m within the FUT. Maximum frequency deviation ( $\Delta f$ ) of 2 GHz is considered, providing a measurement range and spatial resolution of  $\sim 1.42$  km and 6 m respectively. To support this spatial resolution, a space step of 1 m corresponding to a time step of 5 ns is chosen in the forward simulation model. The linear approximation approach assumes that the BFS at non-correlation locations is exactly known. However, that may not be the case in a practical scenario. Hence, while simulating the measured BGS, the BFS at the non-correlation locations is considered to be around 10.8 GHz with an uncertainty of  $\pm 3$  MHz and the local BGS is considered to be Lorentzian with 30 MHz FWHM. The pump-probe frequency offset ( $f_d$ ) is tuned from 10.3 GHz to 11.3 GHz in steps of 1 MHz and the amplified probe is calculated for each  $f_d$ , using Eqs. (7) and (8). The result of this calculation is expected to be measured in the experiment. These values are calculated for two scenarios - one when the BFS at the correlation peak position ( $f_{B0}$ ) is close (10.82 GHz) to that at non-correlation locations and the other when it is very different (11.00 GHz) from that at non-correlation locations. The BFS of the FUT within the width of the correlation peak ( $\sim 6$  m) is assumed to be uniform in both cases. These results are shown in blue (dashed) lines in Figs. 2(a) and 2(b).

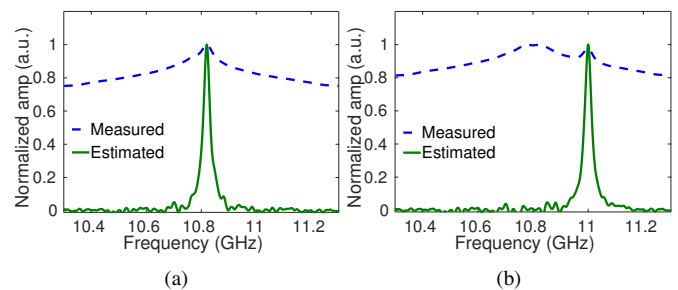


Fig. 2. Perturbation corresponding to a BFS of (a) 10.82 GHz and (b) 11.00 GHz is simulated at 50 m with 10.8 GHz BFS at non-correlation locations. Blue (dashed) curve represents the measured BGS which is simulated by generating a correlation peak at defect location. Green (solid) curve represents the estimated local BGS using the linear approximation approach.

Once the expected amplified probe is generated, the linear approximation method discussed above is used to estimate the BGS at the correlation peak position in each case. The estimated local BGS at the correlation peak position with a BFS of 10.82 GHz and 11.00 GHz are shown in Figs. 2(a) and 2(b) respectively in green (solid) lines. Note that for the estimation, the BFS is assumed to be uniform at all the non-correlation locations (10.8 GHz).

The estimated BGS traces resemble a Lorentzian with 30 MHz FWHM and the peak of the same are found to be

consistent with the BFS chosen at the correlation peak location for both the cases where the BFS at correlation peak location ( $f_{B0}$ ) is close to (Fig. 2(a)) and very different (Fig. 2(b)) from that at the non-correlation locations. The noise observed in the estimated BGS traces is due to the uncertainty considered in the BFS at the non-correlation locations.

### B. BFS estimation with perturbation at different locations

In order to test the robustness of the algorithm, the expected BGS from an experiment is simulated by varying the BFS at the correlation peak position from 10.5 GHz to 11.1 GHz with the BFS at non-correlation locations to be around 10.8 GHz with an uncertainty of  $\pm 3$  MHz. The BGS is estimated using the linear approximation approach in each case and the corresponding BFS at the correlation peak locations is measured from these estimates. The mean error in the estimated BFS is computed by repeating the BFS estimation process with 20 BFS profiles at non-correlation locations with an uncertainty of  $\pm 3$  MHz around 10.8 GHz using Monte Carlo analysis. The same is repeated when correlation peak is positioned at 50 m, 500 m and 950 m over 1 km long FUT. The obtained mean error in the estimated BFS are shown in Fig. 3. The error in the

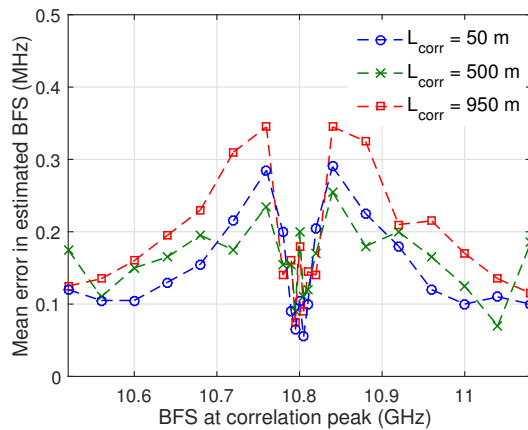


Fig. 3. Mean error in the estimated BFS for correlation peak generated at different locations and with different BFS at the correlation peak position. 20 realizations of BFS profiles at non-correlation locations are considered using Monte Carlo analysis.

estimated BFS is observed to be maximum when the BFS at the correlation peak position is about 40 MHz away from that at non-correlation locations (10.8 GHz) and the error is found to be reducing as the BFS at the correlation peak position is different from that at the non-correlation locations. For the range of BFS considered ( $\pm 300$  MHz which corresponds to a strain of  $6 \mu\epsilon$  considering the strain sensitivity of  $50 \text{ kHz}/\mu\epsilon$  [20]), the maximum error observed in the estimated BFS is around 0.35 MHz. This corresponds to an error of  $7 \mu\epsilon$  in the estimated strain. It may be noted that the error in the estimated BFS depends on the uncertainty in the BFS at non-correlation locations. The above results demonstrate that the linear approximation approach can be used to accurately estimate BFS in a BOCDA system within an error of 0.35 MHz for perturbations at different locations across the FUT and also for different BFS at correlation peak position. However, the linear approximation technique has the following limitations.

### C. BFS estimation using $2f_m$ component of $P_{probe}$

We recently proposed a novel BOCDA technique based on external phase modulation [14], [21] which enables simultaneous BFS measurements at multiple locations. In this technique, both the pump and the probe are modulated with multiple FM signals with different modulation frequencies simultaneously. As a result, multiple correlation peaks are generated at locations decided by the chosen modulation frequencies. This helps in detecting perturbations at multiple locations simultaneously. As in the case of the conventional BOCDA system, the measured BGS is quite broad due to contributions from non-correlation locations in the case of the external phase modulation-based BOCDA as well, thereby limiting the maximum measurable strain. We investigated the feasibility of using the linear approximation approach to estimate the BFS accurately in case of multiple correlation locations. There is one significant difference here - the DC component cannot uniquely identify the BFS at multiple locations [14] and hence the strength of the DC component of  $P_{probe}$  cannot be used to construct the BGS. The amplified probe is periodic with a fundamental frequency of  $2f_m$ . Hence, in order to distinguish multiple locations, we need to use the strength of the corresponding  $2f_m$  component to construct the BGS at a particular correlation peak position. This can be done in the forward model as,

$$P_{BGS}(f_d) = \sum_{t=dt}^{T_m} P_{probe}(0, t, f_d) \exp[-j2\pi(2f_m)t] \quad (9)$$

In order to validate the above method, a defect is simulated at 50 m with a BFS of 10.82 GHz where a correlation peak is generated. The parameters considered are same as those discussed in the results for DC case (Fig. 2). The expected BGS from an experiment is simulated by formulating the linear equations considering the  $2f_m$  component of the  $P_{probe}$ . Fig. 4 shows the expected BGS from the experiment in blue (dashed) lines and the estimated BGS using linear approximation in green (solid) lines. The estimated BGS does not resemble

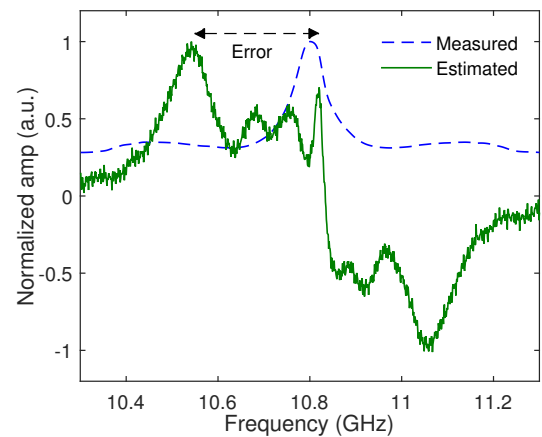


Fig. 4. An event which corresponds to a BFS of 10.82 GHz is simulated at 50 m with 10.8 GHz BFS at other locations. Blue (dashed) curve represents the sample BGS which is simulated by generating a correlation peak at defect location. Green (solid) curve represents the estimated BGS using the linear approximation approach. The strength of the  $2f_m$  component of the  $P_{probe}$  is considered for the estimation.

the typical BGS expected. A local maxima is observed in the estimated BGS at the expected BFS (10.82 GHz). However, the global maxima of the estimated BGS is very different from the expected BFS leading to a large error in the BFS estimation. The BFS estimation is repeated by generating correlation peak at different locations on the FUT and also for different values of BFS at the correlation peak position. In all the cases, the error in the estimated BFS is very large. Note that the strength of the  $2f_m$  component is simulated using Eq. (9), where the right side is a complex number. However, an experiment with direct detection is not expected to measure the phase of the  $2f_m$  component. Hence, the linear approximation approach cannot be used when the strength of the  $2f_m$  component of the amplified probe is considered for the estimation of BFS. An alternative algorithm to overcome this issue is discussed in the following section.

#### IV. GRADIENT DESCENT METHOD TO ESTIMATE BFS

The problem to be solved is a one-dimensional problem as we are interested in estimating the BFS at the correlation peak position only. Hence, we propose a simple gradient descent method [22] for BFS estimation. In this section, we discuss the implementation details of the gradient descent method to accurately estimate the BFS at the correlation peak position even when the strength of the  $2f_m$  component of  $P_{probe}$  is used for BFS estimation.

A key limitation in the linear approximation approach above is that the approximate formula of Eq. (7) is valid only for small gain values corresponding to relatively low pump power levels (in the order of 10 mW). When we use power levels in the order of 100 mW, the small gain approximation may not be valid. To illustrate this, we have simulated the BGS with a probe power of 1 mW and different pump power levels. The mean BFS of the fiber is considered to be 10.8 GHz and that at the correlation location (at 500 m) is considered to be 10.88 GHz. The BGS obtained using exact formula (Eqs. (7) and (8)) for pump power of 10 mW and 100 mW are shown in Figs. 5(a) and (b) respectively.

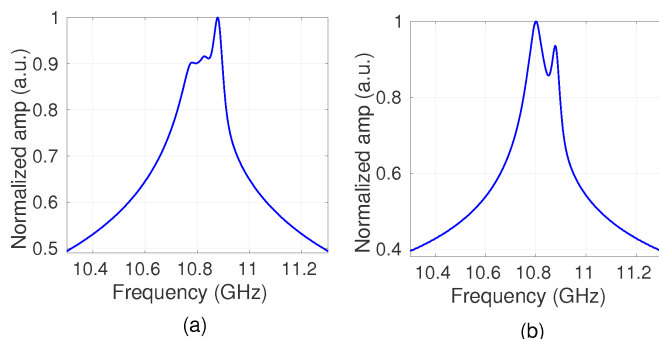


Fig. 5. BGS obtained through simulations for a pump power of (a) 10 mW and (b) 100 mW using exact formula (Eq. (6)).

As seen from Figs. 5(a) and (b), the BGS obtained using a pump power of 10 mW is different from that obtained using 100 mW. We further verified that for a lower pump power of 10 mW the BGS obtained using the approximate formula of

Eq. (7) matches with that obtained using the exact formula of Eq. (6). In case of 100 mW pump power, the BGS obtained using approximate formula does not match with the BGS using exact formula as small gain approximation is not valid. In the simulations discussed in this paper, we have considered a pump power of 100 mW and probe power of 1 mW. Hence, we use Eqs. (6) and (8) for computation of BGS in the simulations discussed below.

#### A. Error function

In this method, we numerically simulate  $P_{BGS}$  using Eqs. (6) and (8) assuming a specific value of BFS ( $f_{BO}$ ) at the correlation peak position. While simulating  $P_{BGS}$ , BFS at non-correlation locations is considered to be known and uniform as in the previous case. We then define an error function  $Q$  considering the measured BGS obtained from experiments (denoted as  $\mathcal{P}_{BGS}$ ) as shown in Eq. (10), such that  $Q$  is minimum when the guess value of BFS matches with the actual BFS at that location.

$$Q(f_{BO}) = \sum_{f_d} \left[ |P_{BGS}(f_d, f_{BO})|^2 - |\mathcal{P}_{BGS}(f_d)|^2 \right]^2 \quad (10)$$

Blue (dashed) and green (solid) curves in Fig. 6 show the error function  $Q$  for varying  $f_{BO}$  when a correlation peak is generated at 500 m which has a BFS of 11.1 GHz without any noise and with a noise corresponding to 5 dB SNR in  $P_{probe}$  respectively. The BFS at the non-correlation locations is considered to be 10.8 GHz with an uncertainty of  $\pm 3$  MHz. The global minimum of the error function  $Q$  occurs when

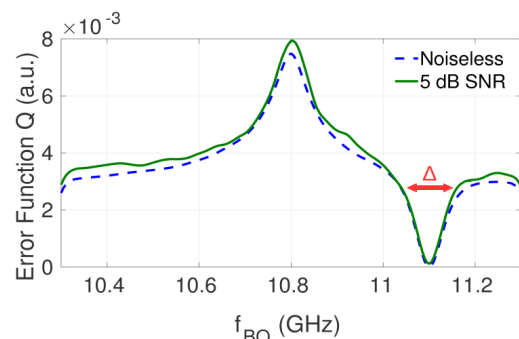


Fig. 6. Error function,  $Q$  for varying initial frequency  $f_{BO}$  when the BFS at the correlation peak position is 11.1 GHz and the BFS at non-correlation locations is 10.8 GHz. Blue (dashed) curve represents noiseless case and green (solid) curve represents case with 5 dB SNR in  $P_{probe}$ .  $\Delta$  indicates the estimated width of the global minimum valley.

$f_{BO}$  is 11.1 GHz which is the BFS at the correlation peak position. We can initialize  $f_{BO}$  to a value and start changing  $f_{BO}$  such that the error function is reduced thereby reaching the actual BFS. However, the error function is non-convex and hence randomly initializing  $f_{BO}$  and moving towards reducing error function may lead to local minima. This is overcome by repeating the above process with multiple initial values and the resultant  $f_{BO}$  value with the lowest error function represents the BFS at the correlation peak position. The number of

initial guesses to be used in the gradient descent algorithm is computed using Eq. (11).

$$\text{Number of initial guesses} = \frac{\text{Desired BFS range}}{\Delta} \quad (11)$$

where  $\Delta$  is the estimated width of the global minimum valley as shown in Fig. 6. For the simulations, we used the range of BFS as 1 GHz.

### B. Gradient descent algorithm

The above mentioned process of moving towards reducing error function and finding the actual BFS can be formulated as an optimization problem shown in Eq. (12), which can be solved using gradient descent method [22] as:

$$f'_{BO} = \underset{f_{BO}}{\text{argmin}} Q(f_{BO}) \quad (12)$$

The principle of the gradient descent method is to move in a direction opposite to the gradient of error function in order to find a local minima. This method is implemented to accurately estimate BFS in a BOCDA system. The expression for the gradient of the error function  $Q$  is shown in Eq. (13). The algorithm used for the gradient descent method for BFS estimation is shown in the Appendix.

$$Q'(f_{BO}) = \frac{\partial Q}{\partial f_{BO}} = \sum_{x \in \text{corr. location}} \sum_{f_d} 2 \left[ |P_{BGS}(f_d, f_{BO})|^2 - |P_{BGS}(f_d)|^2 \right] \times 2 \left\{ \frac{P_{BGS}(f_d, f_{BO}) dt}{T_m} \sum_{t=dt}^{T_m} P_{probe}(0, t, f_d) \frac{P_{pump} dz}{A_{eff} (\frac{\Delta v_B}{2})^2} - 2g_0(f_{BO} - f(x, t - (x/v_g))) \right\} \left( 1 + \left( \frac{f_{BO} - f(x, t - (x/v_g))}{\Delta v_B/2} \right)^2 \right)^2 \quad (13)$$

The convergence of the gradient descent method when the correlation peak is generated at 500 m which has a BFS of 11.1 GHz and with a BFS of 10.8 GHz at non-correlation locations is shown in Fig. 7 with the help of error function  $Q$ . As a specific example,  $f_{B0}$  is initialized to 10.84 GHz and it

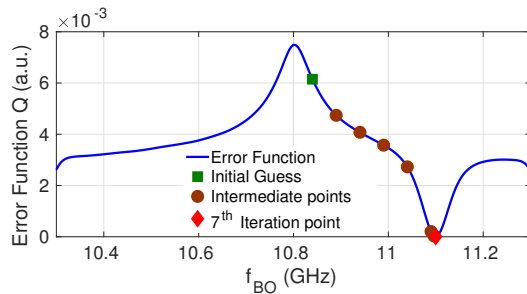


Fig. 7. Blue (solid) curve is the error function  $Q$  for varying  $f_{BO}$  when the BFS at the correlation peak position is 11.1 GHz and the BFS at non-correlation locations is 10.8 GHz. Gradient descent method is used to estimate BFS. Green square is the initial value for  $f_{B0}$  (10.84 GHz), brown circles are the intermediate points and red diamond is the final estimated BFS (11.0998 GHz) after 7 iterations of gradient descent method.

can be observed that using gradient descent method  $f_{B0}$  has reached a value with minimum error function corresponding to the true BFS (11.0998 GHz) within an error of 0.2 MHz in 7 iterations.

### C. BFS estimation in the absence of noise

In order to validate the gradient descent method, the measured BGS is simulated with the same parameters as discussed in Section 3. The correlation peak is simulated at different locations within the FUT and with different BFS at the correlation peak position. The BFS at non-correlation locations is considered to be around 10.8 GHz with an uncertainty of  $\pm 3$  MHz. The gradient descent method is used to estimate the BFS in each case. The error in the estimated BFS for one realization of BFS profile with uncertainty at non-correlation locations is shown in Fig. 8. Here the DC component of the  $P_{probe}$  is considered for estimation. The maximum error observed in

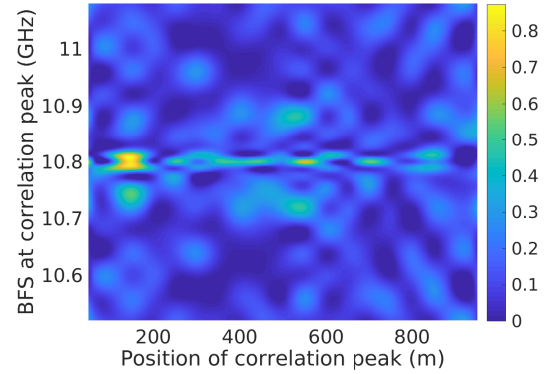


Fig. 8. Error in the estimated BFS for correlation peak generated at different locations and with different BFS at the correlation peak position using gradient descent method. Here strength of the DC component of the  $P_{probe}$  is used for the estimation.

the estimated BFS is around 0.8 MHz. It can be noted that the error shown in Fig. 8 is estimated with only one realization of BFS profile at non-correlation locations. The mean error which is estimated by implementing Monte Carlo analysis for BFS profile at non-correlation locations with uncertainty is much smaller ( $< 0.4$  MHz as can be seen from Fig. 10).

We then proceed to validate the gradient descent algorithm to estimate BFS when the  $2f_m$  component of the  $P_{probe}$  is used for estimation.  $P_{BGS}$  and  $Q'(f_{BO})$  are modified accordingly to account for the  $2f_m$  component. Fig. 9 shows the error in the estimated BFS using  $2f_m$  component with the same parameters used in DC case of Fig. 8. The maximum error observed is around 2.3 MHz which is much lower than that observed with the linear approximation approach (Fig. 4). It can be noted that the error shown in Fig. 9 is estimated with only one realization of BFS profile at non-correlation locations. Hence, the gradient descent method can be used to accurately estimate BFS in a BOCDA system even in the scenario where strength of the  $2f_m$  component of  $P_{probe}$  is considered in order to monitor perturbations at multiple locations simultaneously.

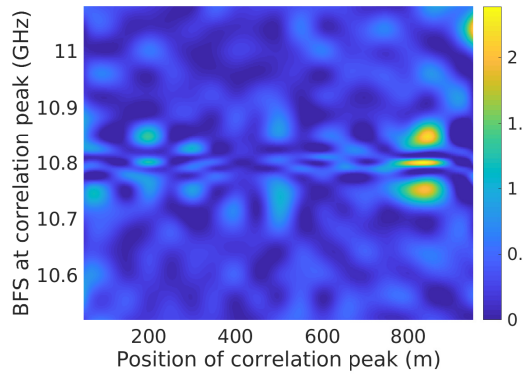


Fig. 9. Error in the estimated BFS for correlation peak generated at different locations and with different BFS at the correlation peak position using gradient descent method. Here strength of the  $2f_m$  component of the  $P_{probe}$  is used for the estimation.

#### D. BFS estimation in the presence of noise

##### Using DC component of $P_{probe}$ :

In order to examine the robustness of the gradient descent method in the presence of noise due to power fluctuations, the amplified probe power  $P_{probe}$  at the pump end is considered with different signal-to-noise ratios (SNR). The correlation peak is generated at 500 m for all the cases. The parameters are similar to those mentioned in Section 3. The measured BFS is simulated for different BFS values at correlation peak position and for  $P_{probe}$  with different SNR values. The BFS at non-correlation locations is considered to be around 10.8 GHz with an uncertainty of  $\pm 3$  MHz. The BFS is estimated using the gradient descent method in each case.

It may be noted that presence of noise in the measured probe power increases the number of local minimas in the error function. The  $\Delta$  (estimated width of the global minimum valley as denoted in Fig. 6) is observed as 100 MHz for DC case in the worst case scenario of 5 dB SNR. Hence, the gradient descent method is repeated with 10 initial values computed using Eq. (11). The final  $f_{BO}$  with minimum error function is considered as estimated BFS. The mean error in the estimated BFS is computed by repeating the same with 20 BFS profiles at non-correlation locations with an uncertainty of  $\pm 3$  MHz around 10.8 GHz and 20 noise profiles for  $P_{probe}$  using Monte Carlo analysis. The obtained mean error in the estimated BFS while considering the strength of the DC component of  $P_{probe}$  is shown in Fig. 10. The results with noiseless case are also shown for comparison.

In the cases without noise and with an SNR of 20 dB, the mean error is maximum when the BFS at the correlation peak position is close to that at the non-correlation locations and it is found to be reducing as the BFS at the correlation peak position is far from that at the non-correlation locations. The worst case value for error observed in these two cases is around 0.4 MHz. With decrease in SNR, the mean error is found to be increasing even when the BFS at correlation peak location is far from that at non-correlation locations. The maximum error in the estimated BFS with an SNR of 5 dB is less than 0.85 MHz.

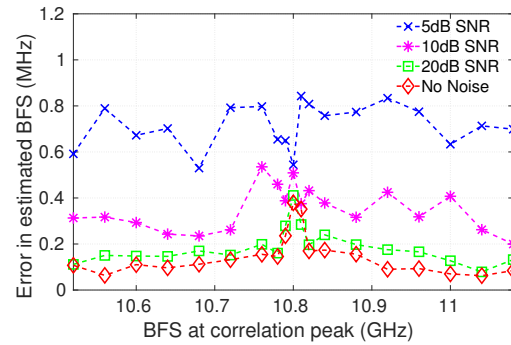


Fig. 10. Mean error in the estimated BFS using gradient descent method for correlation peak generated at 500 m with different SNR in  $P_{probe}$  and with different BFS at the correlation peak position. 20 realizations of BFS profiles at non-correlation locations and 20 realizations of different noise profiles are considered using Monte Carlo analysis. Here the strength of the DC component of  $P_{probe}$  is considered for estimation.

##### Using $2f_m$ component of $P_{probe}$ :

We then proceed to the gradient descent algorithm results in the presence of noise when the strength of  $2f_m$  component is considered for the BFS estimation. The gradient descent method is used to estimate BFS when the correlation peak is generated at 500 m with different BFS and with different SNR for amplified probe power. The  $\Delta$  is observed as 50 MHz for  $2f_m$  case in the worst case scenario of 5 dB SNR. Hence, the gradient descent method is repeated with 20 initial values computed using Eq. (11). The mean error in the estimated BFS is computed by repeating the gradient descent method with 20 BFS profiles at non-correlation locations and 20 noise profiles for  $P_{probe}$  using Monte Carlo analysis. The obtained mean error in the estimated BFS are shown in Fig. 11. The

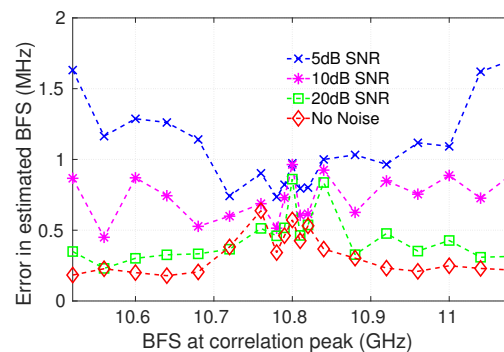


Fig. 11. Mean error in the estimated BFS using gradient descent method for correlation peak generated at 500 m with different SNR in  $P_{probe}$  and with different BFS at the correlation peak position. 20 realizations of BFS profiles at non-correlation locations and 20 realizations of different noise profiles are considered using Monte Carlo analysis. Here the strength of the  $2f_m$  component of  $P_{probe}$  is considered for estimation.

maximum error observed in noiseless case is around 0.6 MHz whereas, with an SNR of 20 dB it is 0.8 MHz. With a decrease in SNR the error increases and with an SNR of 5 dB the error is approximately 1.7 MHz even when the BFS at the correlation peak position is 300 MHz away from that at non-correlation locations. This corresponds to measuring a strain of  $6 \mu\epsilon$  with an error of  $34 \mu\epsilon$ . Hence, the gradient descent

method is robust in the BFS estimation even in the presence of large perturbation at correlation location. From the above results, it is evident that the gradient descent method works well even when the  $2f_m$  component of  $P_{probe}$  is used which is helpful to monitor multiple locations simultaneously. It is observed that in case of DC and  $2f_m$ , it takes a total of about 22 and 52 iterations (on average), respectively, to estimate BFS when an SNR of 5 dB is considered.

We extend the simulations to larger BFS uncertainty at non-correlation locations, the corresponding results are shown in Table I. The correlation peak is positioned at 500 m. In case

TABLE I  
ERROR IN THE BFS ESTIMATION WITH GRADIENT DESCENT METHOD WITH LARGER UNCERTAINTIES OF BFS AROUND MEAN CENTER FREQUENCY (10.8 GHz) AT NON-CORRELATION LOCATIONS.

Case	True BFS at correlation peak (GHz)	Uncertainty in BFS at non-correlation locations (MHz)	Error in estimated BFS (MHz)
DC	10.805	3	0.740
DC	10.805	10	1.312
DC	11.1	3	0.569
DC	11.1	10	0.689
$2f_m$	10.805	3	0.830
$2f_m$	10.805	10	3.242
$2f_m$	11.1	3	0.995
$2f_m$	11.1	10	1.604

of DC measurement, the error in the estimated BFS is less than 1.5 MHz. In case of  $2f_m$  measurement, the error in the estimated BFS is relatively larger.

Another important consideration for the performance evaluation of the algorithms presented above is the computational processing time. The BFS estimation is achieved over a processing time in the order of ten seconds for both the linear approximation approach as well as the gradient descent approach. To compute the gradient or error function, we need to compute  $P_{BGS}(f_b)$  at many different beat frequencies. However, all these computations can be done in parallel using GPUs thereby reducing the processing time. Computational complexity for one iteration is  $O(N_{f_m} N_L N_{f_b})$  where  $N_{f_m}$  is the number of time steps used for one time period ( $1/f_m$ ),  $N_L$  is the number of space discretizations along the length of the fiber and  $N_{f_b}$  is the number of beat frequencies used to get BGS.

### E. BFS estimation with experimental data

We then proceed to validate the gradient descent method for BFS estimation using the experimental data. A schematic diagram of the experimental setup used is shown in Fig. 12. A narrowband laser (linewidth 25 kHz) at a wavelength of 1560 nm is used as the light source. The output of the laser is modulated using an external phase modulator (bandwidth 12 GHz), which is driven by the sum of two sinusoidal FM signals generated from an arbitrary waveform generator (AWG - Keysight M8195A). The output of the phase modulator is filtered using a bandpass filter (BPF<sub>1</sub> - Finisar WaveShaper 1000S) to extract the desired frequency modulated optical signals which are subsequently split into pump and probe waves. The pump lightwave after amplification is launched

from one end of the FUT consisting of a 1 km long fiber (Fiber 1) followed by a 100 m long fiber (Fiber 2). The probe lightwave on the other arm is passed through 13.4 km long delay fiber so that the correlation peak generated within the FUT corresponds to non-zeroth order interaction. The delayed probe is amplified, frequency shifted by the Brillouin frequency ( $f_B$ ) using an electro-optic modulator (EOM, bandwidth 12 GHz) in carrier suppressed configuration and is launched from the other end of the FUT. The frequency modulated pump and probe interact in the FUT and generate a correlation peak at location determined by the  $f_m$  frequency. The amplified probe is filtered using a fiber Bragg grating to extract the Brillouin Stokes component and is detected using a 45 MHz photo receiver. Lock-in detection at  $2f_m$  frequency is performed using an electrical spectrum analyzer (ESA - R&S FSV30) in zero-span mode.

Two correlation peaks are generated simultaneously - one at 588 m and the other at 1005 m by driving the external phase modulator using modulation frequencies of 75 kHz and 80 kHz respectively [21]. The frequency deviation ( $\Delta f$ ) used is 2 GHz each. The pump-probe frequency offset is varied from 10.7 GHz to 10.9 GHz. The strength of the corresponding  $2f_m$  components (150 kHz and 160 kHz) of the amplified probe are captured which are the measured BGS shown as blue (dashed) curves in Figs. 13(a) and 13(b) respectively. The BFS at both the correlation peak locations for the measured BGS are estimated using the gradient descent method. The corresponding error functions computed through Eq. (10) are shown in Figs. 13(c) and 13(d) respectively.

The error functions have a minima at frequencies of 10.7945 GHz and 10.794 GHz respectively indicating them to be the BFS values at the two locations which are closely matching with the actual BFS values (10.796 GHz and 10.793). We simulated the BGS with the obtained BFS values at the correlation peak positions and are shown as green (solid) curves in Figs. 13(a) and 13(b) respectively. The simulated BGS traces are consistent with those measured through experiments with an error of 1.5 MHz and 1 MHz in BFS values at the two locations. It took a total of about 15 iterations (from 4 initial guesses) to estimate BFS as the frequency range of BFS was only 200 MHz and hence, we needed to search only a smaller span. These results demonstrate that the gradient descent method is a promising approach to accurately estimate BFS at the correlation peak position.

## V. CONCLUSION

The Brillouin gain spectrum (BGS) obtained in a conventional BOCDA consists of contributions from non-correlation locations. In such a scenario, fitting a narrow region around the peak to estimate the Brillouin frequency shift (BFS) may work only for cases where the BFS at the correlation location is close to the BFS at the non-correlation locations. In this paper, we explore two new approaches for the accurate estimation of BFS at the correlation location irrespective of its value with respect to the BFS at the non-correlation location in a BOCDA system. A simple linear approximation of the Brillouin gain is first proposed and is found to provide BFS estimation

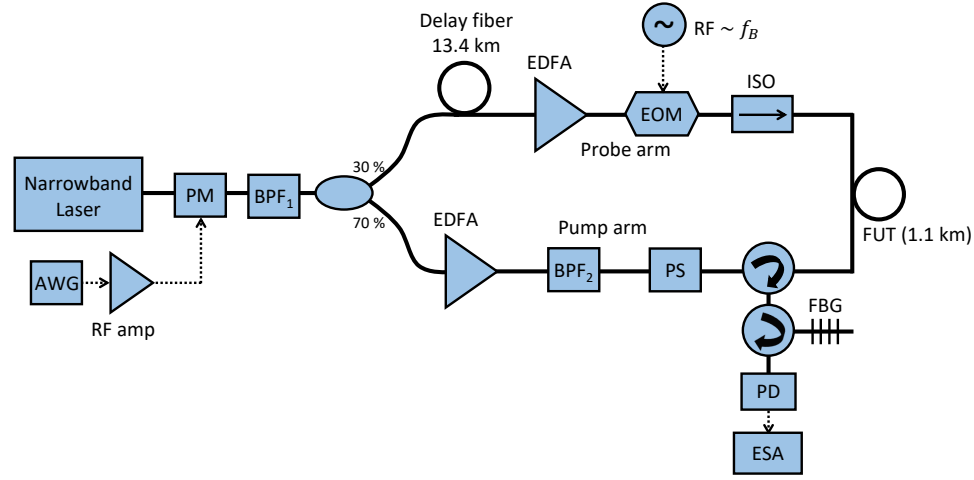


Fig. 12. Schematic of the experimental setup used; PM: Phase modulator; AWG: Arbitrary waveform generator; BPF: Bandpass filter; EDFA: Erbium-doped fiber amplifier; EOM: Electro-optic modulator; ISO: Optical isolator; PS: Polarization scrambler; FBG: Fiber Bragg grating; PD: Photo detector; ESA: Electrical spectrum analyzer.

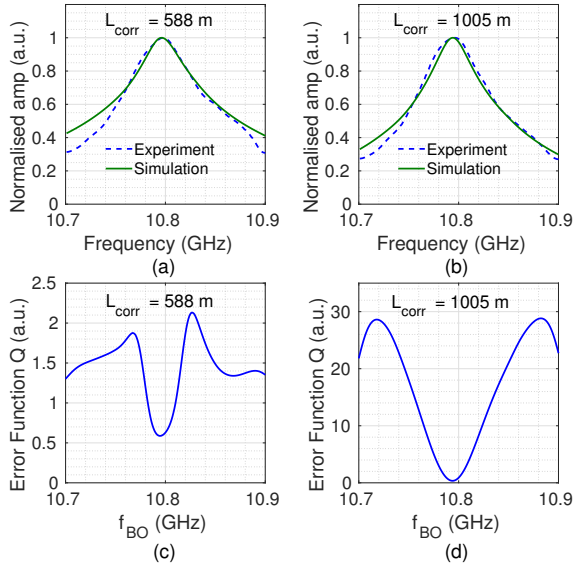


Fig. 13. Blue (dashed) and green (solid) curves in (a) and (b) represent the BGS traces obtained from experiments and simulation respectively using the  $2f_m$  component of  $P_{probe}$  when correlation peak is generated at (a) 588 m and (b) 1005 m. The corresponding error functions obtained while estimating BFS using gradient descent method are shown in (c) and (d).

accuracy well within 1 MHz. However, the utility of such an approximation is found to be limited to measurements based on the DC component. For Brillouin sensor measurements relying on signals at the modulation frequency or its harmonics, we propose a more robust and accurate gradient descent algorithm. We have quantified the performance of the gradient descent algorithm under different SNR regimes and find it to be providing BFS error of less than 1 MHz over 500 MHz frequency range for SNR as low as 5 dB. The simulation results have also been validated through a careful comparison with experimental results.

## APPENDIX

Algorithm to estimate BFS using gradient descent method is given below.

- 1: **Initialize**  $f_{BO}, c$  ▷  $f_{BO}$  is the initial guess
- 2: Gradient Converge = 'false'
- 3: **repeat** ▷ Gradient Descent
- 4:      $f_{old} \leftarrow f_{BO}$
- 5:      $\alpha \leftarrow 5 \times 10^8 / |Q'(f_{old})|$
- 6:     Step Length Converge = 'false'
- 7:     **repeat** ▷ Line Search
- 8:          $f_{new} \leftarrow f_{old} - \alpha Q'(f_{old})$  ▷ Gradient Update
- 9:         **if**  $Q(f_{old}) - Q(f_{new}) \geq c\alpha |Q'(f_{old})|^2$  **then**
- 10:             Step Length Converge = 'true'
- 11:              $f_{old} \leftarrow f_{new}$
- 12:         **else**
- 13:              $\alpha \leftarrow \alpha/2$
- 14:         **end if**
- 15:     **until** Step Length Converge
- 16:     **if**  $\frac{|Q(f_{BO}) - Q(f_{new})|}{|Q(f_{BO})|} \leq 10^{-5}$  **then**
- 17:         Gradient Converge = 'true'
- 18:     **end if**
- 19:      $f_{BO} \leftarrow f_{new}$
- 20: **until** Gradient Converge
- 21: Repeat the method for multiple initial guesses.
- 22: Output the  $f_{BO}$  with minimum  $Q$ .

## ACKNOWLEDGMENT

The authors would like to acknowledge the financial support from Ministry of Human Resource Development (MHRD), Department of Science and Technology (DST), Department of Electronics and Information Technology (DeitY) and Office of the Principal Scientific Advisor, Government of India, and thank Dr. K V Reddy, PriTel Inc., USA for providing the optical amplifier used in our experiments.

## REFERENCES

- [1] T. Horiguchi, T. Kurashima, and M. Tateda, "A technique to measure distributed strain in optical fibers," *IEEE Photon. Technol. Lett.*, vol. 2, no. 5, pp. 352–354, 1990.
- [2] T. Kurashima, T. Horiguchi, and M. Tateda, "Distributed-temperature sensing using stimulated Brillouin scattering in optical silica fibers," *Opt. Lett.*, vol. 15, no. 18, pp. 1038–1040, 1990.
- [3] M. Nikles, L. Thévenaz, and P. A. Robert, "Simple distributed fiber sensor based on Brillouin gain spectrum analysis," *Opt. Lett.*, vol. 21, no. 10, pp. 758–760, 1996.
- [4] M. N. Alahbabi, Y. T. Cho, and T. P. Newson, "150-km-range distributed temperature sensor based on coherent detection of spontaneous Brillouin backscatter and in-line Raman amplification," *J. Opt. Soc. Am. B*, vol. 22, no. 6, pp. 1321–1324, 2005.
- [5] X. Bao and L. Chen, "Recent progress in Brillouin scattering based fiber sensors," *Sensors*, vol. 11, no. 4, pp. 4152–4187, 2011.
- [6] K. Y. Song and K. Hotate, "Distributed fiber strain sensor with 1-kHz sampling rate based on Brillouin optical correlation domain analysis," *IEEE Photon. Technol. Lett.*, vol. 19, no. 23, pp. 1928–1930, 2007.
- [7] A. Zadok, Y. Antman, N. Primerov, A. Denisov, J. Sancho, and L. Thevenaz, "Random-access distributed fiber sensing," *Laser Photonics Rev.*, vol. 6, no. 5, pp. L1–L5, 2012.
- [8] K. Hotate and T. Hasegawa, "Measurement of Brillouin Gain Spectrum Distribution along an Optical Fiber Using a Correlation-Based Technique—Proposal, Experiment and Simulation," *IEICE Trans. Electron.*, vol. E83-C, no. 3, pp. 405–412, 2000.
- [9] K. Hotate, "Brillouin Optical Correlation-Domain Technologies Based on Synthesis of Optical Coherence Function as Fiber Optic Nerve Systems for Structural Health Monitoring," *Appl. Sci.*, vol. 9, no. 1, p. 187, 2019.
- [10] M. Nikles, L. Thevenaz, and P. A. Robert, "Brillouin gain spectrum characterization in single-mode optical fibers," *J. Lightw. Technol.*, vol. 15, no. 10, pp. 1842–1851, 1997.
- [11] J. H. Jeong, K. Lee, K. Y. Song, J.-M. Jeong, and S. B. Lee, "Differential measurement scheme for Brillouin optical correlation domain analysis," *Opt. Express*, vol. 20, no. 24, pp. 27 094–27 101, 2012.
- [12] K. Y. Song, Z. He, and K. Hotate, "Optimization of Brillouin optical correlation domain analysis system based on intensity modulation scheme," *Opt. Express*, vol. 14, no. 10, pp. 4256–4263, 2006.
- [13] B. Somepalli, D. Venkitesh, U. Khankhoje, and B. Srinivasan, "Deconvolution Algorithm for Accurate Estimation of Brillouin Frequency in Brillouin Optical Correlation Domain Analysis," in *26th International Conference on Optical Fiber Sensors*. Optical Society of America, 2018, p. ThE20.
- [14] B. Somepalli, D. Venkitesh, and B. Srinivasan, "Simultaneous Multi-point Sensing through External Phase Modulation based Brillouin Optical Correlation Domain Analysis," in *Asia Communications and Photonics Conference*. Optical Society of America, 2017, pp. M2A–3.
- [15] K. Hotate, "Fiber distributed Brillouin sensing with optical correlation domain techniques," *Opt. Fiber Technol.*, vol. 19, no. 6, pp. 700–719, 2013.
- [16] K. Y. Song, Z. He, and K. Hotate, "Effects of intensity modulation of light source on Brillouin optical correlation domain analysis," *J. Lightw. Technol.*, vol. 25, no. 5, pp. 1238–1246, 2007.
- [17] R. W. Boyd, *Nonlinear Optics*. Academic press, 2008.
- [18] G. P. Agrawal, *Nonlinear Fiber Optics*. Academic press, 2007.
- [19] B. Wang, X. Fan, Y. Fu, and Z. He, "Dynamic strain measurement with kHz-level repetition rate and centimeter-level spatial resolution based on Brillouin optical correlation domain analysis," *Opt. Express*, vol. 26, no. 6, pp. 6916–6928, 2018.
- [20] L. Thévenaz, "Brillouin distributed time-domain sensing in optical fibers: state of the art and perspectives," *Frontiers of Optoelectronics in China*, vol. 3, no. 1, pp. 13–21, 2010.
- [21] B. Somepalli, D. Venkitesh, and B. Srinivasan, "Multi-point Dynamic Strain Sensing using External Phase Modulation-based Brillouin Optical Correlation Domain Analysis," *arXiv preprint arXiv:1807.10640*, 2018.
- [22] J. Nocedal and S. J. Wright, *Numerical optimization 2nd*. Springer, 2006.